Surfactant adsorption by total internal reflection Raman spectroscopy. Part III: adsorption onto cellulose

David A. Woods[a], Jordan Petkov[b], Colin D. Bain[a,*]

[a] *Department of Chemistry, University of Durham, University Science Laboratories, South Road, Durham, DH1 3LE, UK.*
[b] *Unilever Research and Development Laboratory, Port Sunlight, Quarry Road East, Bebington, Wirral, CH63 3JW, UK.*

Abstract

TIR Raman spectroscopy has been used to study the adsorption of surfactants onto cellulose. The cellulose was prepared by Langmuir-Blodgett deposition of trimethylsilylcellulose onto silica followed by removal of the trimethylsilyl groups with acid to generate a hydrophilic surface. The reaction was followed *in situ* with Raman spectroscopy, revealing a two-step hydrolysis. Adsorption isotherms of hexadecyltrimethylammonium bromide (CTAB) and Triton X-100 (TX-100) on hydrophilic cellulose were obtained by TIR Raman scattering under quasi-equilibrium conditions where the bulk concentration was slowly but continuously varied. The isotherms of both surfactants are almost linear, in contrast to the isotherms on hydrophilic silica. The CTAB isotherm shows hysteresis depending on whether the concentration of the surfactant is increasing or decreasing due to a slow adsorption region. A mixture of TX-100 and CTAB shows ideal adsorption, in contrast to adsorption of the same mixture on silica where there is a strong cooperative interaction at low CTAB surface coverage.

Keywords: cellulose, total internal reflection Raman, surfactant adsorption

Contents

*Corresponding author
Email address: c.d.bain@durham.ac.uk (Colin D. Bain)

1. Introduction

Cellulose is the core component of cotton and paper. The adsorption of surfactants onto cellulose is a key step in the cleaning of cotton textiles and in the deinking of paper during recycling. Optimisation of formulations is assisted by an understanding of the thermodynamics and kinetics of adsorption of surfactants onto cellulose, both as pure compounds and as mixtures. Here we use total internal reflection (TIR) Raman spectroscopy to study the adsorption of surfactants onto cellulose both as binary solutions in water and as a ternary mixture. TIR Raman spectroscopy was invented in the 1970s[1, 2] but it is only recently that it has been developed into a powerful, surface-sensitive technique for quantitative studies of adsorption at the solid-liquid interface.[3–7] In Parts 1 and 2 of this series,[4, 5] we demonstrated the use of TIR Raman spectroscopy in the study of the adsorption of pure and mixed surfactants on a silica substrate. While the technique is at its most straightforward when the substrate is transparent and has vibrational bands that do not overlap with those of the adsorbates, TIR-Raman spectroscopy can also be applied successfully to thin

films deposited on transparent substrates even when, as is the case with cellulose, the vibrational spectrum of the thin film strongly overlaps the spectra of the adsorbates of interest.

TIR-Raman exploits the properties of evanescent waves to achieve surface sensitivity and therefore requires the use of surfaces that are flat on the length scale of the wavelength of light. TIR-Raman can be used to study fibrous materials if the material is pressed up against an internal reflection element composed of a high-index material,[8] but quantification is difficult and kinetic studies impractical. Fortunately, there are well-established techniques for preparing thin, flat transparent films of cellulose that are suitable for study by optical and neutron scattering techniques.[9–11] In the work reported here, we first use TIR-Raman spectroscopy to characterise the preparation of a model cellulose surface by hydrolysis of the trimethylsilyl groups in a Langmuir-Blodgett film of hydrophobically modified cellulose. Next we look at the adsorption onto cellulose of the cationic surfactant hexadecyltrimethylammonium bromide (CTAB), which is a commonly used model system. The speed of acquisition of TIR Raman spectra allows us to map the adsorption isotherm much more thoroughly than has been done before. Third, we look at the adsorption of the non-ionic surfactant Triton X-100 (TX-100) onto cellulose. TX-100 is challenging to study because it removes some of the cellulose layer, however the chemical specificity of Raman allows the two different processes—adsorption of surfactant and degradation of the layer—to be followed independently. Finally, we look briefly at a mixed surfactant system, demonstrating the ability of TIR-Raman spectroscopy to distinguish two surfactants in the presence of a strong cellulose signal.

Previous work on cellulose has taken two different approaches to sample preparation. Fibrous cellulose[12, 13]—for example filter paper—has the advantage of replicating real cellulose substrates closely, but the disadvantages that the cellulose surface contains a wide variety of different environments, that *in situ* characterisation of molecules adsorbed to the cellulose is difficult and that adsorption kinetics are likely to be controlled by transport through the fibres rather than by adsorption onto the surface itself. These drawbacks

are overcome with thin, flat cellulose substrates. Such surfaces have allowed the use of a wide range of different experimental methods, including X-ray photoelectron spectroscopy,[14, 15] surface force apparatus,[16] atomic force microscopy,[17] quartz crystal microbalance,[18] ellipsometry[9] and neutron reflectometry[10, 11] as well as the TIR Raman spectroscopy we use here. They are also amenable to quantitative studies of adsorption kinetics under well-defined mass transport conditions.[9]

Two different approaches exist for the preparation of thin cellulose films:[19] Langmuir-Blodgett (LB) deposition and spin coating. The most common approach to LB deposition, developed by Schaub *et al.*,[20] involves the use of the functionalised cellulose derivative trimethylsilyl cellulose (TMSC). The principal advantage of working with TMSC rather than plain cellulose is that—unlike plain cellulose—TMSC can be dissolved in common non-polar solvents such as chloroform, toluene or *n*-hexane. Thin layers of TMSC can then be formed at the air-water interface and transferred onto hydrophobic surfaces such as hydrophobised gold, glass, silicon or mica. Unfunctionalised cellulose can be regenerated by exposure to HCl vapour. The properties of the deposited surface have been characterised extensively by IR spectroscopy, surface plasmon resonance, ellipsometry, surface force measurements and photoelectron spectroscopy,[16, 20, 21] providing thicknesses of 10 Å per layer for TMSC and 4 Å per layer for the regenerated cellulose, showing that the charge on the cellulose chains is minimal (based on the absence of a double-layer force) and that the removal of the TMS groups is essentially complete.

Alternatively, TMSC can be spin-coated onto a substrate such as an anchoring polymer attached to silicon,[9, 22] or directly onto silicon or gold,[14] followed by hydrolysis to remove the TMS groups. Kontturi and coworkers showed that partial hydrolysis was possible and could be controlled by changing the vapour pressure of HCl and the exposure time.[14] Neuman *et al.* showed that it is also possible to spin coat cellulose directly using trifluoroacetic acid as a solvent;[23] the current preferred solvent is N-methylmorpholine-N-oxide (NMMO).[24] Cellulose has to be deposited onto an anchoring polymer—rather

than directly onto silica—with the choice of polymer affecting the thickness of the surface. For all spin-coating processes, a range of experimental parameters can be used to control the film thickness, with typical values being 200–1000 Å.

We used Langmuir-Blodgett deposition of TMSC rather than spin coating, principally because the films produced can be made thinner than those from spin-coating, with much finer control over the thickness of the film. A thin film is important in TIR Raman to minimise the Raman signal from cellulose, which overlaps the surfactant spectra.

The adsorption of CTAB onto cellulose has been studied by both neutron reflectometry[10] and AFM.[17] The two sets of data are not directly comparable since the surfaces were prepared in different ways: the AFM study used unfunctionalised cellulose spin-coated on top of a polymer layer[24] whereas the neutron reflectometry used Langmuir-Blodgett deposition of a hydrophobically modified cellulose to produce hydrophobic and hydrophilic cellulose layers. Measured by neutron reflectometry,p levels of adsorption onto hydrophilic cellulose and hydrophilic silica were similar ($5.9\,\mu\mathrm{mol\,m^{-2}}$), whereas the level of adsorption onto hydrophobic cellulose was roughly a third lower ($3.9\,\mu\mathrm{mol\,m^{-2}}$). Modelling of the neutron data suggested some intermixing between the hydrophobic cellulose and CTAB, whereas the CTAB self-assembled on top of the hydrophilic cellulose. AFM data revealed the formation of admicelles on a hydrophilic cellulose surface.

The adsorption of nonionic surfactants to cellulose has also been studied. Torn *et al.* followed the adsorption kinetics of a variety of ethylene glycol alkyl ether (C_nE_m) surfactants using optical reflectometry.[9] Singh and Notley used AFM to show a mixture of spherical and rodlike micelles for $C_{16}E_8$ and $C_{14}E_6$ on cellulose surfaces.[25] Adsorption of $C_{12}E_6$ and mixtures of CTAB and $C_{12}E_6$ have been investigated by neutron reflectometry.[11] $C_{12}E_6$ appeared to change the structure of both TMS-functionalised and plain cellulose while the original structure was largely recovered on rinsing. In mixtures, the composition of the surface layer on plain cellulose was close to ideal. The surface excess was largely independent of composition on both types of cellulose.

Several authors have studied adsorption of surfactants onto cellulose fibres. Paria *et al.* looked at the adsorption of TX-100, sodium dodecylbenzenesulfonate and CTAB) onto filter paper:[12, 26] the kinetics were generally slow, taking between 5 and 50 min to complete. Alila *et al.* used oxidation of cellulose fibres to control the surface charge and then investigated the adsorption of different chain lengths alkyl trimethylammonium bromide surfactants.[13] The nature of cellulose fibres makes comparison of these results to those obtained on a thin flat cellulose film almost impossible.

2. Experimental

2.1. Materials

Hexadecyltrimethylammonium bromide (Sigma-Aldrich, 99%) was recrystallized three times from acetone/methanol. Triton X-100 (Sigma-Aldrich)—a nonionic surfactant with a branched octylphenyl tail group and a poly(oxyethylene) head group with an average of 9.5 EO units—was used as received. Water was obtained from a Millipore Gradient A-10 filtration unit (18.2 MΩ cm, TOC $<$ 4 ppb). Trimethylsilyl cellulose was synthesised according to the method given in reference 27.

2.2. Raman

The TIR-Raman system has been described in detail elsewhere.[4, 6]. The Raman light is collected with commercial Raman microscope (Ramascope 1000, Renishaw, Wootton-under-edge, UK). The pump laser is a continuous-wave, frequency-doubled solid-state laser (Opus 532, Laser Quantum, Manchester, UK) with a wavelength of 532 nm, typically operated at 0.7 W yielding ∼0.5 W at sample. The beam was gently focused to a diameter of ∼10 µm. A silica hemisphere was used as the substrate for the cellulose to minimize optical aberrations. The angle of incidence at the silica-water interface was 73.0° giving an illuminated region of 30 × 10 µm and a sampling depth for Raman scattering of 103 nm. The incident laser was S polarised (perpendicular to the plane of incidence), since this polarization gives the highest signal levels. The Raman scattered radiation was collected through the fused silica prism with a 50×

ULWD, 0.55 NA objective (Olympus) and directed into the spectrometer. Typically we collected only the y-polarised light (parallel to the incident S light, designated Sy); x-polarised light could also be selected (designated Sx). Data were acquired over a fixed wavenumber range (from 2600 to 3200 cm^{-1}) encompassing the C–H stretching region of the Stokes scattering.

For measurements on quasi-equilibrium systems—using the continuously stirred mixer described later—a continuous set of 10–30 s spectra were acquired. For measurements on the kinetics of adsorption and desorption (presented in the supplementary material) we used 1-s acquisitions. With a 1-s readout time between scans, the overall time resolution is 2 s. The sets of spectra (both quasi-equilibrium and kinetic) were analysed by a chemometric method known as target factor analysis (TFA).[28] The first step in TFA is to decompose the data set into its principal components. The first n components contain orthogonal linear combinations of the water and surfactant spectra while the remaining components are noise. For a pure surfactant solution, $n = 2$: a background component consisting of water and cellulose, and the spectrum of the surfactant. The second step is a coordinate rotation to extract the refined spectra corresponding to the background and the surfactant and their component weights in each of the input spectra. To perform this rotation a pair of target spectra are required that approximate to the refined water and refined surfactant spectra. The target spectrum for the background was acquired at the beginning of each experiment from a cellulose-coated prism in the cell filled with pure water. The target spectrum for the surfactant was obtained by manual subtraction of the background target spectrum from the spectrum of the highest concentration surfactant solution. The component weight of the surfactant spectrum from the TFA was divided by the component weight of the background spectrum to compensate for any drift in the microscope focus or laser power and to account for differences in the acquisition time (so that the longer equilibrium measurements appear on the same scale as the shorter kinetic measurements).

Target Factor Analysis yields component weights that determine the relative contribution of the refined spectra to each raw spectrum in the data set. The

surface excess (in moles m^{-2} of surface) was calibrated from the contribution to the equilibrium Raman spectra from surfactants molecules in bulk solution within the evanescent wave: the number of bulk molecules contributing to the signal is simply the bulk concentration multiplied by the sampling depth. Above the cmc of a pure surfactant solution, the surface excess remains constant and therefore the increase in Raman signal with increasing surfactant concentration may be ascribed to bulk surfactant. Thus, the slope in component weight above the cmc yields a calibration factor to convert component weight into surface excess. Unfortunately, the susceptibility of the cellulose films to removal by surfactant limited our ability to use high enough bulk surfactant concentrations to derive an accurate calibration factor. An alternative approach is to compare the intensities of the surfactant peaks (relative to the water background that acts as an internal reference) with those on bare silica.[4] This comparison neglects the water within the cellulose layer and any alignment differences between the two experiments. Consequently, we have presented the surfactant coverages as a component weight and quoted our best estimate for the conversion to surface excess in the figure captions.

2.3. Wall-jet cell

The sample cell and connecting tubing is illustrated in figure 1. The custom-made glass cell consists of an inner chamber with a volume of 6 mL surrounded by an outer jacket through which temperature-controlled water is passed. A tube allows a thermocouple probe to be inserted into the outer jacket. The top of the sample chamber is capped with a 10-mm diameter silica hemisphere sealed to the chamber with a Viton O-ring. An inlet tube (1-mm inner radius) is positioned 1.8 mm below the hemisphere surface. The cell is designed in the well-defined wall-jet geometry, which ensures that mass transport to the surface is both rapid and well understood.[9]

The cell, the tubing connecting the cell, and all the other glassware used in the experiment was cleaned with a commercial alkaline cleaning agent (Borer 15PF concentrate), then rinsed with copious high-purity water. Prior to the

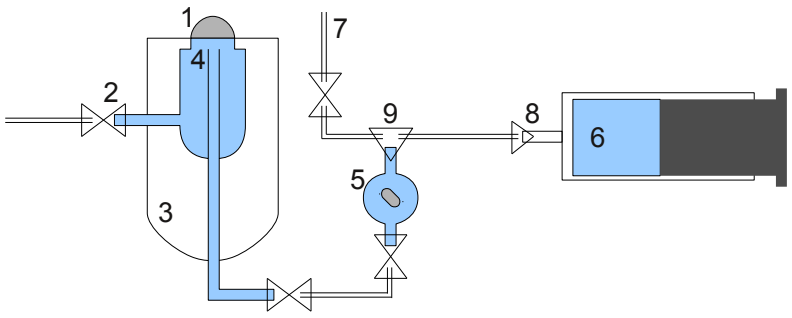

Figure 1: Diagram of the flow cell and connecting tubing. 1) Silica hemisphere, 2) outlet tube, 3) temperature controlled jacket, 4) inlet tube, 5) in-line mixer, 6) 50-mL syringe, 7) outlet to remove air bubbles from the tubing after connecting the syringe, 8) Luer-lock connector between syringe and tubing, and 9) three-way junction. Two touching triangles represent on/off valves.

cellulose coating (described in the next section) fused silica hemispheres were soaked in chromosulfuric acid for at least 4 hours, then rinsed with high purity water. The cellulose-coated prisms were used for at most a single day; the cellulose layer was then stripped off with chromosulfuric acid and the coating process started again from scratch. Between each experiment the cell was flushed with at least 100 mL of high purity water to wash any residual surfactant off the surface.

2.4. Cellulose coating

The sample preparation was based on the work of Penfold *et al.*,[10] with some modifications. The cellulose was coated onto silica hemispheres (10 mm diameter; Global Optics, Bournemouth, UK). The hemisphere was cleaned as described above. The silica surface was hydrophobised by exposure to a 1,1,1,3,3,3-hexamethyldisilazane (purchased from Sigma-Aldrich) atmosphere for >12 h, room temperature, in a dry nitrogen atmosphere and then rinsed with water. TMSC dissolved in dichloromethane at a concentration of 0.7 mg mL^{-1} was spread on the surface of a Langmuir trough (Nima, Coventry, UK) and compressed to a surface pressure of 20 mN m^{-1}. TMSC monolayers were then

transferred to the hemispheres at dipping and withdrawal rate of $5\,\mathrm{mm\,min^{-1}}$ with a 135-s pause at the end of both the dipping and the withdrawal. During the depositions the hemispheres were mounted so that the flat surface was vertical. Each hemisphere was dipped 5 times to produce a layer approximately 30 Å thick (based on literature reports that 10 dippings give a 60-Å thick film)[10]. Since parts of the holder and the hemispherical face of the prism also pass through the surface of the trough and may be coated with TMSC, it is not possible to calculate a transfer ratio. The cellulose layer on the curved surface of the hemisphere is too thin to affect significantly incident light entering the hemisphere.

The LB process produces a hydrophobic cellulose surface. Removal of the TMS groups to produce a hydrophilic surface was carried out within the wall-jet cell by exposure of the samples to a 3.5% solution of HCl for 15 mins, at a flow rate of $0.5\,\mathrm{mL\,min^{-1}}$. We followed the removal of the methyl groups spectroscopically during the acid wash. Following the exposure to acid, the hemispheres were rinsed thoroughly with high purity water. This process deviates from most other work, where the hemisphere is exposed to the vapour above an HCl solution. The cellulose surfaces prepared are uniform (within the 10–30 μm resolution afforded by the laser spot size). The reproducibility in the amount of cellulose deposited is ±20%. Similar variability was observed in thickness measurements from neutron reflectivity.[10, 11]

Figure 2 illustrates schematically how the coated hemisphere is used in the Raman experiment. The refractive index of wet cellulose is intermediate between that of dry cellulose ($n = 1.53$) and water ($n = 1.33$) and is probably not very different from that of silica ($n = 1.46$).[9] Consequently, total internal reflection of the green laser beam takes place at the cellulose-water interface rather than the silica-cellulose interface.

All the surfactant isotherms and kinetics presented here were recorded on the unfunctionalised (hydrophilic) cellulose: we found that the TMS-functionalised cellulose was very readily removed by surfactants (especially TX-100, but also CTAB).

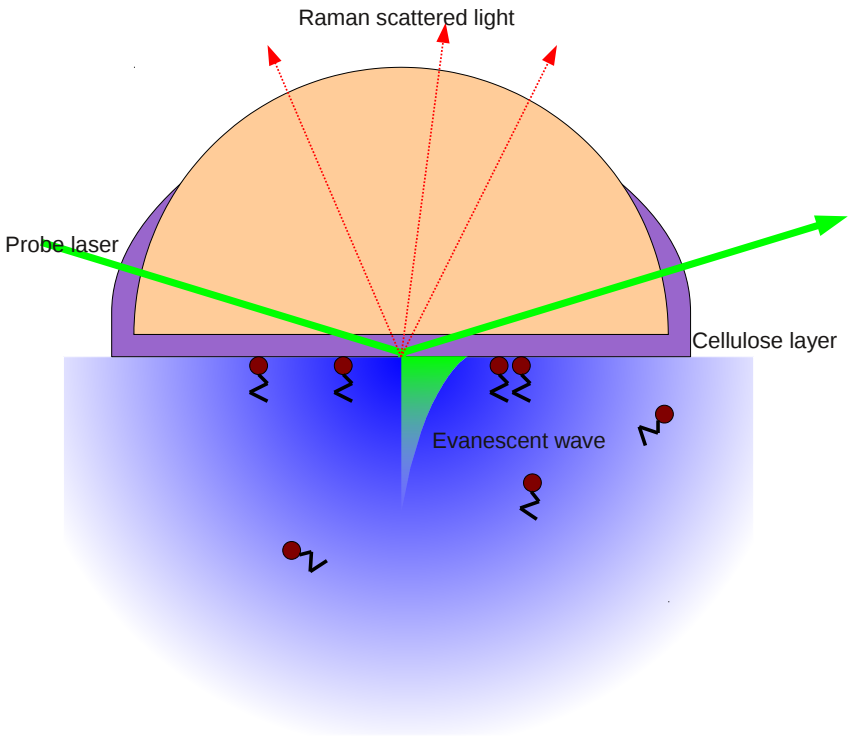

Figure 2: Schematic diagram of the cellulose hemisphere and the Raman probe laser (not to scale).

2.5. Continuous stirred mixer

Conventionally, adsorption isotherms are acquired by a stepwise increase in concentration, waiting for an equilibration time and then acquiring data at a fixed concentration before stepping to the next higher concentration. In this work we used a different procedure in which the concentration in the cell was slowly but continuously varied and Raman spectra were acquired continuously. This 'quasi-equilibrium' approach provides a much larger number of data points in a shorter total time. Provided that the surface equilibrates quickly on the time scale of the change in concentration, then an equilibrium isotherm will be obtained. To test whether equilibrium has been achieved, isotherms are acquired with increasing and decreasing concentration: hysteresis in the isotherm is a hallmark of slow kinetics.

To obtain a smoothly varying concentration profile at the surface of the hemisphere a continuous stirred mixer was installed in the inlet tube to the wall-jet cell (see figure 1). The mixer is a flat cylinder with a volume of 8.3 mL with an inlet and an outlet (leading to the cell) on opposite sides. A magnetic stirrer bar is sealed inside it and rotates rapidly (>200 rpm). The mixer is initially filled with one solution, and a second solution is then pumped in at a constant rate. We will refer to experiments where a surfactant is added to water as "in" experiments and the inverse—where a surfactant is diluted with water—as "out" experiments. The mixed can also be used to effect a change in the composition of mixtures of surfactants.

The concentration, $[A]$, within the mixer varies according to a simple first-order rate equation. For an "in" experiment

$$[A] = [A]_{\text{in}} \left(1 - e^{-\frac{R}{V}t}\right) , \tag{1}$$

while for an "out" experiment

$$[A] = [A]_0 e^{-\frac{R}{V}t} , \tag{2}$$

where $[A]_{\text{in}}$ and $[A]_0$ are the inlet and initial concentrations respectively, R is the pumping rate, V the volume of the mixer and t the time since pumping started.

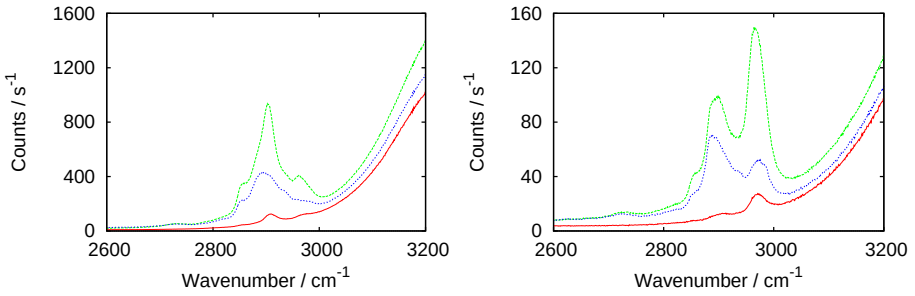

(a) (b)

Figure 3: TIR Raman spectra in the C–H stretching region of a hydrophobised hemisphere (red solid line), after coating with TMS-cellulose (green dashed line) and after hydrolysis of the TMS groups (blue dotted line): (a) Sy and (b) Sx polarisation. Acquisition time = 300 s. In each case the surface is in contact with water.

The time taken for the solution to travel from the outlet of the mixer to the sample surface was determined to be 100 s at a pumping rate of 0.5 mL min^{-1} (and was scaled accordingly at other pumping rates). The acquisition time of each spectrum was 0.17–0.5 min, which is short compared to the characteristic time over which the concentration varies: V/R = 17 min. The characteristic time for surfactant to cross the diffusion layer adjacent to the interface in our wall-jet flow cell is ∼4 s,[4] therefore we do not expect the final transport step of diffusion to the surface to be significant when using the mixer. The time taken to record a complete isotherm (a single "in" or "out" measurement) is the syringe volume divided by the flow rate, so for a 50-mL syringe and a flow rate of 0.5 mL min^{-1}, the isotherm takes 100 mins to record. A detailed description of the in-line mixer and the validation of the technique will be presented elsewhere.

3. Removal of -Si(CH$_3$)$_3$ from cellulose

Throughout this section we will use TMS to represent the -Si(CH$_3$)$_3$ group, whether it is bonded to cellulose or to the silica substrate. Polarisation-resolved spectra were acquired of a hemisphere hydrophobised with disilazane, after coating with hydrophobic cellulose and following hydrolysis with aqueous HCl. Fig-

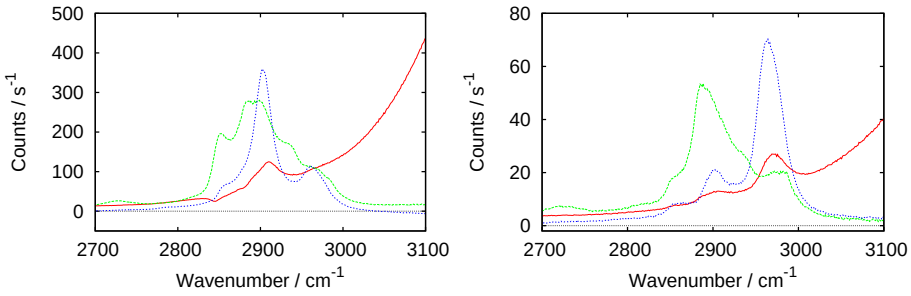

(a) (b)

Figure 4: The three components of the TIR Raman spectra shown in figure 3: water and TMS groups on silica (red solid line), plain cellulose (green dashed line) and TMS groups on cellulose (blue dashed line). (a) Sy and (b) Sx polarisation.

ure 3 shows the Sy and Sx-polarised spectra. For the purposes of this paper the differences between the polarisations are not important except to note that the relative intensities of peaks differ and so some changes are easier to see in one polarisation than the others.

In order to follow the hydrolysis of the TMS-cellulose in real time by target factor analysis, we decompose the spectra into the three components shown in figure 4:

1. water/hydrophobic silica background, including the TMS peak from the hydrophobic coating;
2. unfunctionalised cellulose (the final state of the cellulose with the water/hydrophobic silica background subtracted);
3. TMS covalently attached to cellulose, generated by subtraction of the cellulose spectrum from the TMS-cellulose spectrum.

The difference spectrum between the two forms of cellulose—before and after the acid rinse—is very similar to the difference spectrum between hydrophobised silica and clean silica in water, except that the latter is shifted $\sim 5\,\mathrm{cm}^{-1}$ to higher wavenumber (Figure 5). This similarity between the two difference spectra shows that only TMS groups are lost during the acid rinse, and no cellulose.

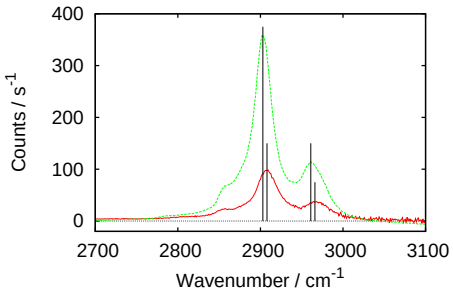

Figure 5: Comparison of spectra for -Si$(CH_3)_3$ groups from functionalised silica (solid red lines) and TMS cellulose (dashed green lines), Sy polarisation, acquisition time = 300 s. Vertical lines indicate approximate peak positions. The peak at 2903 cm^{-1} (TMS-cellulose) or 2908 cm^{-1} (functionalised silica) is the symmetric CH_3 stretch; the peak at 2961 cm^{-1} (TMS-cellulose) or 2966 cm^{-1} (functionalised silica) is the asymmetric CH_3 stretch.[15]

The shift in wavenumber reflects differences in chemical environment and allows the TMS groups on silica and cellulose to be identified independently. The TMS on groups on silica do not appear to be lost during the acid rinse: their contribution to the overall spectrum remains constant. To confirm that the TMS groups attached to silica are not removed by acid, we performed the acid rinse on a hydrophobised, but not cellulose-coated, hemisphere; there was no change between the spectra recorded before and after the acid rinse.

The hydrolysed cellulose spectrum still shows a small peak at 2970 cm^{-1} from the TMS groups (this is seen especially clearly in the Sx polarisation, figure 4(b)), indicating that some TMS groups remain after hydrolysis. The peak appears at a higher wavenumber than both the TMS removed from cellulose and the TMS on silica, indicating that the TMS groups on cellulose that survive the acid wash are in a different chemical environment from those removed. The area of the 2970 cm^{-1} peak permits an estimate of the unhydrolysed fraction of TMS groups of 5 to 10%.

Based on the integral of the spectra, the amount of TMSC deposited by the Langmuir-Blodgett process was observed to vary by up to ±30% from its average value but the fraction of TMS groups removed from the TMSC by acid

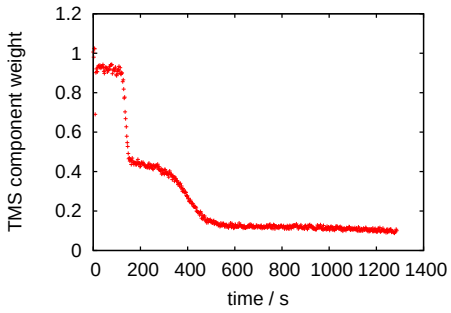

Figure 6: Kinetics of removal of TMS from cellulose. Sy polarisation, 1 s acquisition time per point, flow rate of HCl solution = 0.5 mL min^{-1}. Only the TMS component is plotted; the cellulose/water component varied by less than 20% over the course of the experiment.

hydrolysis remained constant.

Figure 6 shows the kinetics of hydrolysis. Inspection of the abstract principal components showed that only two factors were needed for the target factor analysis: a TMS factor and a factor accounting for the constant background of water and cellulose. The hydrolysis proceeds in two steps: a rapid initial removal of approximately half of the TMS groups, followed by a slower removal of the remaining TMS. These kinetics suggest that the TMS groups exist in two forms, with a difference in accessibility to acid. The two-step kinetics seen here are very reproducible however the fraction of the TMS groups removed in the first step varies between 0.2 and 0.7; the kinetic run shown in Fig. 6 is in the middle of the range.

The hydrolysis of TMS cellulose by HCl vapour has previously been followed by XPS, ATR-IR,[14, 15] and static contact angle measurements.[15] The XPS data suggested complete removal of the TMS groups, from the part of the film accessible to XPS (approximately the top 5 nm).[14] The TMSC film was removed from the vapour after varying exposure times, rinsed with water and then analysed *ex situ*. Only four measurements were taken throughout the complete hydrolysis process, so it was not possible to identify the two-stage kinetics seen here. Very recently the hydrolysis has been followed *in situ* by

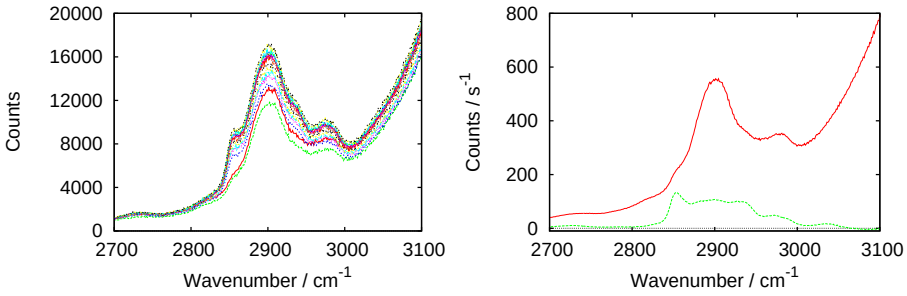

(a) (b)

Figure 7: (a) Example spectra (Sy polarisation) and (b) component spectra used in the analysis of the CTAB isotherm shown in figure 8. For part (b) the red solid line shows the water and cellulose background component while the green dashed line is the CTAB component. For part (a) each spectrum shows a 30 s acquisition and only every 10th spectrum is shown. The spectra in part (a) are illustrative so the time-stamps are not individually labelled.

X-ray reflectivity,[29] and fitted to a first-order rate equation with respect to TMSC remaining. The acquisition rate was much slower than possible with TIR-Raman (5 data points over ∼6 mins), so the 2-step process could easily have been missed, if hydrolysis by vapour proceeds in the same way as hydrolysis by solution.

4. CTAB

An adsorption isotherm of CTAB on hydrophilic cellulose was obtained with the inline mixer to vary continuously the sub-surface concentration of CTAB. Figure 7 shows examples of the raw data that generate a CTAB isotherm, together with the two components used in the target factor analysis of the data. When the sets of spectra are processed with TFA, they yield the isotherms shown in figure 8. The limiting surface excess from the isotherm was estimated to be $\sim 2\,\mu\text{mol}\,\text{m}^{-2}$ from the slope of the CTAB component weight above the cmc (see Experimental Section), however this value is very approximate since measurements at higher concentrations are required for an accurate calibration of the component weights. For this reason we have plotted the isotherm

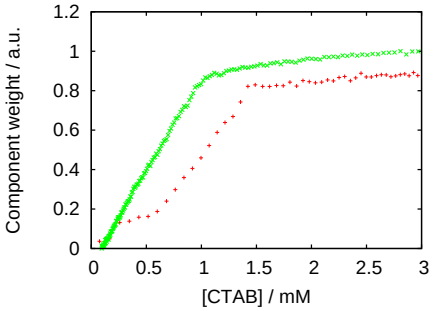

Figure 8: Adsorption isotherm of CTAB on hydrophilic cellulose, expressed as CTAB component weight normalised to water. Red '+' represent an "in" measurement; green '×' represent an "out" measurement. The flow rates were $0.3\,\mathrm{mL\,min^{-1}}$. The CTAB solution was 5 mM concentration. Each point is from a 30 s spectrum. A component weight of 1.0 is estimated to represent a surface coverage of 2.0–2.8 $\mu\mathrm{mol\,m^{-2}}$.

in terms of component weight only. An alternative method for estimating the surface excess is to compare the intensities of the CTAB component adsorbed to cellulose and to silica surface, using the water component as an internal reference. The CTAB component measured on cellulose is approximately half the size of that on silica. Given that the adsorbed amount on the silica has been measured as $5.5\,\mu\mathrm{mol\,m^{-2}}$,[30] the estimated surface excess on cellulose is about $2.8\,\mu\mathrm{mol\,m^{-2}}$, which is a somewhat higher than the value estimated from bulk surfactant contribution above the cmc but lower than that determined by neutron reflection.[10]

The isotherms in figure 8 show hysteresis between the measurements taken with CTAB concentration increasing (red +), and those with CTAB concentration decreasing (green ×). Changing the flow rate, R, from 0.3 to $0.5\,\mathrm{mL\,min^{-1}}$ had little effect on the hysteresis. Due to the exponential dependence of concentration with time (equations 1 and 2), the rate of change of concentration in the low concentration region is slowest during the "out" runs and therefore the "out" kinetics are closer to the equilibrium isotherm than the "in". This interpretation is supported by the difference in the apparent cmcs of the "out" and "in" measurements: for the "out" measurement the onset of desorption appears

at 0.9 mM, matching the known cmc of CTAB, whereas for the "in" measurement the limiting surface excess is not reached until the bulk concentration reaches 1.5 mM, which is well above the cmc.

Figure 8 shows a plateau in the surface excess in the in measurement at low concentration. A similar plateau has been observed in the adsorption of CTAB on silica an ascribed to and electrostatic interaction between the positively charged surfactant and the negatively charged surface.[31] For CTAB adsorption on cellulose, however, we believe the plateau seen in the "in" measurement is primarily a kinetic feature since it is not present in the "out" isotherm. The delay in adsorption during the "in" measurement is similar to the slow adsorption region reported for cationic surfactants on silica,[32, 33] which is attributed to the nucleation of surface aggregates. Slow adsorption has not previously been reported on a cellulose surface, but the adsorption kinetics of cationic surfactants on cellulose have not been as extensively studied.

The "out" isotherm is close to linear with concentration. Lattice based isotherms (for example the Langmuir or Frumkin isotherms) cannot provide a good fit to such a linear region. It is unusual for isotherms be so linear and the interpretation is unclear. A linear isotherm could potentially arise from a combination of the wide variety of different adsorption sites present on cellulose, which promote adsorption at low surface excess as the favourable sites are filled first, and the favourable interactions between adjacent CTAB molecules which promote adsorption at higher surface excesses.

The only previous adsorption isotherm of CTAB on cellulose was obtained by Penfold *et al.* using neutron reflection. They reported similar levels of adsorption for CTAB on cellulose and silica ($\sim$6 μmol m^{-2}). Due to the limited availability of neutron beamtime they were only able to measure four concentrations below the cmc, with a minimum concentration of 0.1 mM. When replotted on a linear concentration scale, their data shows $\mathrm{d}\Gamma/\mathrm{d}c$ decreasing slightly with increasing concentration. They saw no evidence of a plateau at low concentrations, consistent with the plateau in Figure 8 being a kinetic rather than thermodynamic effect. They found that adsorption and desorption of CTAB

did not change the thickness of the cellulose layer. For thin films (thickness much less than the penetration depth of the evanescent wave), TIR-Raman is sensitive only to the total amount of adsorbed cellulose and not to thickness.

Kinetics of adsorption for CTAB on hydrophilic cellulose are shown in the supplementary material (Figure S.1a). CTAB of the specified concentration was flushed directly into the cell at a flow rate of $0.5\,\mathrm{mL\,min^{-1}}$. The rates of adsorption increase gradually with increasing concentration before levelling out above the cmc. At the highest concentrations (4 and 10 mM), adsorption is complete within 20 s, which is much faster than reported on filter paper.[26] Adsorption onto cellulose is roughly 3 times slower than onto silica.[4]

The kinetics of desorption are also shown in the supplementary material (Figure S.1b). The rates of desorption vary little with concentration. Most of the data are for initial concentrations above or near the cmc. Desorption does not commence until the subsurface concentration drops below the cmc; an initial concentration above the cmc therefore affects the time delay before desorption begins more than the desorption process itself.

5. TX-100

An isotherm for the adsorption of TX-100 onto cellulose is shown in figure 9(a). The component spectra are shown in figure 9(b). The TX-100 caused loss of a small amount of cellulose, which is also shown in figure 9(a). The loss of cellulose is a kinetic—rather than an equilibrium—property and should be linked to time rather than the bulk TX-100 concentration (TX-100 concentration increased with time during the "in" measurement and decreases with time on the "out" measurement. The similarity of the TX-100 isotherm in the 'in" and "out" measurements shows that the loss of a small amount of cellulose does not significantly affect the adsorption properties.

We were able to obtain a reasonable straight line increase in TX-100 signal above the cmc (using a higher concentration than in figure 9 and not shown here), giving a limiting surface excess for TX-100 ($1.2\,\mu\mathrm{mol\,m^{-2}}$) approximately a quarter of than on pure silica ($4.3\,\mu\mathrm{mol\,m^{-2}}$).[4] However, comparison of the

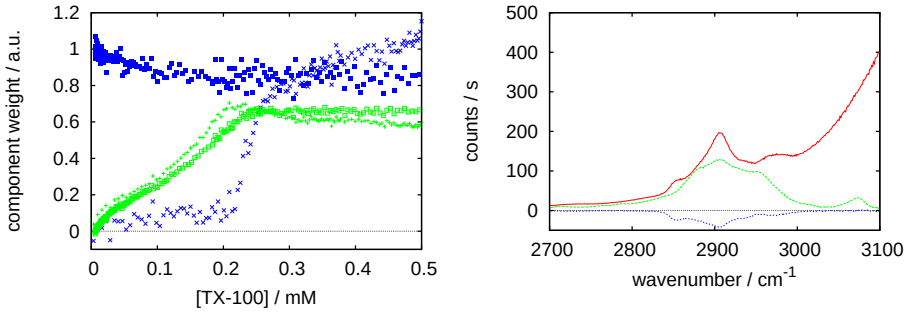

(a) (b)

Figure 9: (a) TX-100 adsorption isotherm, expressed as component weight normalised to water. TX-100 is shown in green ("in" measurement: +, "out" measurement: ⊡); change in cellulose signal during the experiment is shown in blue ("in" measurement: ×, "out" measurement: ■). Acquisition times were 10 s for the first 100 spectra and 30 s for the remainder; the flow rate was 0.5 mL min^{-1} and the surfactant solution 0.6 mM concentration. For TX-100, a component weight of 1.0 corresponds to a surface excess of approximately 4 µmol m^{-2}. The change in cellulose signal cannot readily be interpreted as an absolute value. (b) Components used in analysis of the TX-100 isotherm. The background spectrum is shown as solid red lines, the TX-100 spectrum is shown as dashed green lines and the change in cellulose is shown as dotted blue lines.

relative sizes of the TX-100 component for adsorption on silica and cellulose (normalised to water in both cases) yields a much larger value for the maximum surface excess of around $2.6\,\mu\mathrm{mol\,m^{-2}}$ (∼60% of that onto silica). This discrepancy suggests that in the TFA there may be a small amount of mixing of the TX-100 component and the component ascribed to the loss of cellulose. We therefore prefer the higher value as the best estimate of the surface excess. The most important difference between the adsorption of TX-100 onto silica[4] and cellulose is the shape of the isotherm: the isotherm on silica is a step function, while on cellulose the isotherm shows a smooth increase with concentration. Our observations contrast with the results of Singh and Notley who reported that the $C_{16}E_8$ isotherm was more step-like on cellulose, and saw little change in the isotherm of $C_{14}E_7$.[25] In our earlier work on adsorption at silica[4] we attributed the step function to a strong interaction parameter promoting the formation of two phases. The smooth isotherm on cellulose suggests a reduction in the interaction between adjacent TX-100 molecules, possibly because aggregation is disrupted by a rougher surface or due to incorporation of TX-100 into the cellulose layer.

There is a propensity for TX-100 to remove the hydrophilic cellulose from the hydrophobic silica surface. The loss of cellulose is variable from experiment to experiment. During the recording of a single adsorption isotherm ("in" or "out") the loss of hydrophilic cellulose is sufficiently slow that the adsorption isotherm is not greatly affected. Greater damage is caused by the three-phase line moving across the sample surface, for example when emptying and refilling the cell, which makes acquiring a large series of adsorption kinetics difficult. TMS-cellulose is particularly labile in TX-100 which prevented us from acquiring any reproducible isotherms from TMSC.

Only a very limited range of adsorption and desorption kinetics have been measured, due to the removal of the cellulose film by TX-100 described above. Examples of both adsorption and desorption kinetics are shown in the supplementary material (Figure S.2). Too few adsorption kinetics were acquired to draw useful conclusions. Desorption kinetics are quick and the rate of desorp-

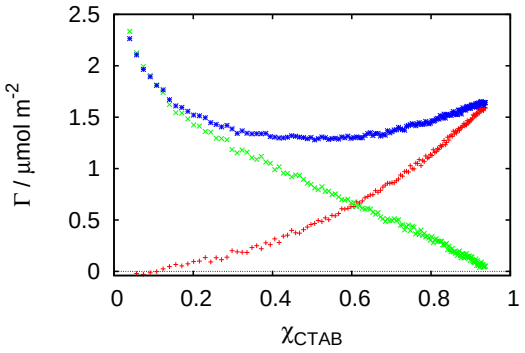

Figure 10: Adsorption of a mixture of TX-100 (green ×) and CTAB (red +) onto cellulose, 2 mM total concentration, with respect to surface excess (given as a mole fraction of CTAB). Total surface excess is also shown (blue *). Recorded while sweeping from pure TX-100 to CTAB with 0.3 mL min^{-1} flow rate, Sy polarisation, 30 s acquisition time. There is considerable uncertainty in the absolute surface excesses, due to the uncertainty in the calibration factors used when analysing the pure surfactant isotherms.

tion is essentially independent of concentration. As with the CTAB desorption kinetics this concentration independence is expected and shows that desorption does not start until the bulk concentration has dropped below the cmc.

6. Mixed systems

In a previous paper[5] we have studied the adsorption of mixtures of CTAB and TX-100 mixed systems onto silica, measuring the surface excesses for both surfactants at varying bulk composition with a constant 2 mM concentration. Target factor analysis was used to distinguish the two species on the surface. Here, we perform the same experiment on a cellulose surface (Figure 10), but using the inline mixer (with 2-mM CTAB replacing 2-mM TX-100) rather than a series of discrete compositions. TFA worked well with two components representing the surfactants and third representing the hydrophobic silica and the cellulose layer, demonstrating that the presence of the overlapping Raman spectrum of cellulose does not prevent quantitative analysis of mixed surfactant adsorption. One of the most striking features of adsorption onto silica is a two-fold

increase in adsorbed amount caused by the presence of small (2%) mole fractions of CTAB.[5] The origin of this cooperative effect is likely to be the interaction between the positively charged CTAB and the negatively charged silica surface. On cellulose there is no such promotion of adsorption at low CTAB mole fractions. In contrast there is a decrease in adsorption compared to the pure surfactants throughout most the composition range. Although CTAB and TX-100 do interact favourably, as shown by work on the micellisation[34] and our work on silica, it is possible that if the TX-100 adsorbs inside the cellulose surface the opportunity for mixed aggregates to form is limited (this is plausible if TX-100 is able to remove the cellulose layer). The formation of mixed micelles in solution would then decrease the chemical potential of the surfactants and hence decrease the adsorbed amount.

7. Conclusions

We have demonstrated the use of TIR-Raman spectroscopy for measuring adsorption onto a model polymer surface (cellulose), and shown that the signal from the cellulose surface does not prevent the determination of the amount of adsorbed surfactants in both pure and mixed systems. TIR-Raman is sensitive enough to follow adsorption kinetics with a 2-s time resolution.

The main experimental difficulty in performing experiments on cellulose deposited on a hydrophobic surface is the propensity of surfactants—especially TX-100—to remove the cellulose during experiments. The TMS-functionalised cellulose film is particularly easily removed. Performing a range of kinetics measurements is especially difficult, since the process of emptying and refilling the cell after each measurement removes the surface especially quickly.

The adsorption isotherms of both CTAB and TX-100 on cellulose are close to linear, in contrast to the isotherms on silica which are strongly influenced by electrostatic interactions with the substrate (in the case of CTAB) and intermolecular interactions between surfactants in surface micelles (for both surfactants). The linearity of the adsorption isotherms on cellulose may arise from a balance of two effects: the heterogeneity of the adsorption sites, which promotes

adsorption at low coverages, and the intermolecular interactions that promote adsorption at high coverages.

The surfactant isotherms were acquired continuously under quasi-equilibrium conditions in which slow adsorption/desorption kinetics are manifested by hysteresis between isotherms taken with increasing and decreasing surfactant concentrations. The CTAB isotherm exhibited pronounced hysteresis. A 'slow adsorption region' below the cmc has previously been implicated in the adsorption of CTAB on silica and assigned to formation and reorganisation of surface aggregates.[32, 33] One feature of the inline mixer is that the rate of change of concentration is higher nearer the beginning of the experiment than the end. Consequently, the measurement taken with decreasing concentration is closer to equilibrium in the concentration range below the cmc than is the measurement with increasing concentration.

A mixed adsorption isotherm was acquired at 2-mM total concentration for comparison with adsorption on silica. The mixed layers on cellulose do not show the strong interaction between components that is displayed on silica, with no evidence of cooperative behaviour.

We are also able to follow the removal of TMS functional groups from cellulose during the preparation of the model surface. Although the initial and final states of the cellulose film have previously been studied in considerable detail, only TIR-Raman spectroscopy has the time resolution to follow the hydrolysis as it takes place, revealing a previously unseen two-step hydrolysis.

8. Acknowledgements

DAW thanks Unilever R&D, Port Sunlight for funding through a CASE award. We would also like to thank the referees for their helpful suggestions.

[1] T. Ikeshoji, Y. Ono, T. Mizuno, Total reflection raman spectra; raman scattering due to the evanescent wave in total reflection, Appl. Opt. 12 (10) (1973) 2236–2237. doi:10.1364/AO.12.002236.
URL http://ao.osa.org/abstract.cfm?URI=ao-12-10-2236

[2] R. Iwamoto, M. Miya, K. Ohta, S. Mima, Total internal reflection raman spectroscopy, Journal of Chemical Physics 74 (9) (1981) 4780–4790. doi:10.1063/1.441757.

[3] C. Lee, C. D. Bain, Raman spectra of planar supported lipid bilayers, Biochimica et Biophysica Acta (BBA) - Biomembranes 1711 (1) (2005) 59–71. doi:DOI:10.1016/j.bbamem.2005.02.006.
URL http://www.sciencedirect.com/science/article/B6T1T-4FJXJMT-2/2/93f22ac34db1efcf888965b77886009e

[4] D. A. Woods, J. Petkov, C. D. Bain, Surfactant adsorption kinetics by total internal reflection raman spectroscopy. 1. pure surfactants on silica, The Journal of Physical Chemistry B (2011) ASAP (doi: 10.1021/jp201338s)doi:10.1021/jp201338s.

[5] D. A. Woods, J. Petkov, C. D. Bain, Surfactant adsorption kinetics by total internal reflection raman spectroscopy. 2. ctab and triton x-100 mixtures on silica, The Journal of Physical Chemistry B (2011) ASAP (doi: 10.1021/jp201340j)doi:10.1021/jp201340j.

[6] E. Tyrode, M. W. Rutland, C. D. Bain, Adsorption of ctab on hydrophilic silica studied by linear and nonlinear optical spectroscopy, Journal of the American Chemical Society 130 (51) (2008) 17434–17445. arXiv:http://pubs.acs.org/doi/pdf/10.1021/ja805169z, doi:10.1021/ja805169z.
URL http://pubs.acs.org/doi/abs/10.1021/ja805169z

[7] D. Beattie, M. Lidström Larsson, A. R. Holmgren, In situ total internal reflection raman spectroscopy of surfactant adsorption at a mineral surface, Vibrational Spectroscopy 41 (2) (2006) 198–204, 6th Australian Conference on Vibrational Spectroscopy. doi:DOI:10.1016/j.vibspec.2006.02.003.
URL http://www.sciencedirect.com/science/article/B6THW-4JN2NSX-4/2/622262a80c8b4cea8488bd435777eb00

[8] P. R. Greene, C. D. Bain, Total internal reflection raman spectroscopy, Spectroscopy Europe (2004, Aug/Sep) 8–15.

[9] L. H. Torn, L. K. Koopal, A. de Keizer, J. Lyklema, Adsorption of nonionic surfactants on cellulose surfaces: Adsorbed amounts and kinetics, Langmuir 21 (17) (2005) 7768–7775.
URL http://pubs3.acs.org/acs/journals/doilookup?in_doi=10.1021/la051102b

[10] J. Penfold, I. Tucker, J. Petkov, R. K. Thomas, Surfactant adsorption onto cellulose surfaces, Langmuir 23 (16) (2007) 8357–8364.

[11] I. Tucker, J. Petkov, J. Penfold, R. K. Thomas, Adsorption of nonionic and mixed nonionic/cationic surfactants onto hydrophilic and hydrophobic cellulose thin films, Langmuir 36 (11) (2010) 8036–8048. doi:10.1021/la1000057.

[12] S. Paria, C. Manohar, K. C. Khilar, Adsorption of anionic and non-ionic surfactants on a cellulosic surface, Colloids and Surfaces A: Physicochemical and Engineering Aspects 252 (2–3) (2005) 221–229.

[13] S. Alila, S. Boufi, M. N. Belgacem, D. Beneventi, Adsorption of a cationic surfactant onto cellulosic fibers i. surface charge effects, Langmuir 21 (18) (2005) 8106–8113. arXiv:http://pubs.acs.org/doi/pdf/10.1021/la050367n, doi:10.1021/la050367n.
URL http://pubs.acs.org/doi/abs/10.1021/la050367n

[14] E. Kontturi, P. C. Thüne, J. W. H. Niemantsverdriet, Cellulose model surfaces – simplified preparation by spin coating and characterization by x-ray photoelectron spectroscopy, infrared spectroscopy, and atomic force microscopy, Langmuir 19 (14) (2003) 5735–5741. arXiv:http://pubs.acs.org/doi/pdf/10.1021/la0340394, doi:10.1021/la0340394.
URL http://pubs.acs.org/doi/abs/10.1021/la0340394

[15] T. Mohan, R. Kargl, A. Doliska, A. Vesel, S. Köstler, V. Ribitsch, K. Stana-Kleinschek, Wettability and surface composition of partly and fully regenerated cellulose thin films from trimethylsilyl cellulose, Journal of Colloid and Interface Science 358 (2) (2011) 604–610.

doi:DOI:10.1016/j.jcis.2011.03.022.
URL http://www.sciencedirect.com/science/article/B6WHR-52C8FWB-6/2/e551b376af09d1d7df0e44265ac30cc2

[16] M. Holmberg, J. Berg, S. Stemme, L. Ödberg, J. Rasmusson, P. Claesson, Surface force studies of langmuir – blodgett cellulose films, Journal of Colloid and Interface Science 186 (1997) 369–381. doi:doi:10.1006/jcis.1996.4657.

[17] S. M. Notley, Direct visualization of cationic surfactant aggregates at a cellulosewater interface, J. Phys. Chem. B 113 (42) (2009) 13895–13897.

[18] T. Tammelin, T. Saarinen, M. Österberg, J. Laine, Preparation of langmuir/blodgett-cellulose surface by using horizonal dipping procedure. application for polyelectrolyte adsorption studies performed with qcm-d, Cellulose 13 (5) (2006) 519–535.

[19] E. Kontturi, T. Tammelin, M. Österberg, Cellulose—model films and the fundamental approach, Chem. Soc. Rev. 35 (2006) 1287–1304.

[20] M. Schaub, G. Wenz, G. Wegner, A. Stein, D. Klemm, Ultrathin films of cellulose on silicon wafers, Advanced Materials 5 (12) (1993) 919–922.

[21] C. Wegner, V. Buchholz, L. Ödberg, S. Stemme, Regeneration, derivatization and utilization of cellulose in ultrathin films, Advanced Materials 8 (5) (1996) 399–402.

[22] C. Geffroy, M. P. Labeau, K. Wong, B. Cabane, M. A. Cohen Stuart, Kinetics of adsorption of polyvinylamine onto cellulose, Colloids and Surfaces A: Physicochemical and Engineering Aspects 172 (1-3) (2000) 47–56. doi:DOI:10.1016/S0927-7757(00)00499-4.
URL http://www.sciencedirect.com/science/article/B6TFR-40TY3R6-5/2/1d0a9028e7b334856e51cad245eb53ff

[23] R. D. Neuman, J. M. Berg, P. M. Claesson, Direct measurement of surface forces in papermaking and paper coating systems, Nordic

Pulp & Paper Research Journal 8 (1) (1993) 96–104. doi:10.3183/NPPRJ-1993-08-01-p096-104.

[24] S. Gunnars, L. Wågberg, M. A. Cohen Stuart, Model films of cellulose: I. method development and initial results, Cellulose 9 (3–4) (2002) 239–249.

[25] S. K. Singh, S. M. Notley, Adsorption of nonionic surfactants (cnem) at the silica-water and cellulose-water interface, The Journal of Physical Chemistry B 114 (46) (2010) 14977–14982. arXiv:http://pubs.acs.org/doi/pdf/10.1021/jp107224r, doi:10.1021/jp107224r.
URL http://pubs.acs.org/doi/abs/10.1021/jp107224r

[26] S. Paria, C. Manohar, K. C. Khilar, Kinetics of adsorption of anionic, cationic, and nonionic surfactants, Industrial & Engineering Chemistry Research 44 (9) (2005) 3091–3098. arXiv:http://pubs.acs.org/doi/pdf/10.1021/ie049471a, doi:10.1021/ie049471a.
URL http://pubs.acs.org/doi/abs/10.1021/ie049471a

[27] M. Kostag, S. Köhler, T. Liebert, T. Heinze, Pure cellulose nanoparticles from trimethylsilyl cellulose, Macromolecular Symposia 294 (2) (2010) 96–106. doi:10.1002/masy.200900095.
URL http://dx.doi.org/10.1002/masy.200900095

[28] E. R. Malinowski, Factor Analysis in Chemistry, 2nd Edition, John Wiley & Sons, 1991.

[29] E. Kontturi, A. Lankinen, Following the kinetics of a chemical reaction in ultrathin supported polymer films by reliable mass density determination with x-ray reflectivity, Journal of the American Chemical Society 132 (11) (2010) 3678–3679, pMID: 20187644. arXiv:http://pubs.acs.org/doi/pdf/10.1021/ja100669w, doi:10.1021/ja100669w.
URL http://pubs.acs.org/doi/abs/10.1021/ja100669w

[30] E. Tyrode, M. W. Rutland, C. D. Bain, Adsorption of ctab on hydrophilic silica studied by linear and nonlinear optical spectroscopy, Journal of the

American Chemical Society 130 (51) (2008) 17434–17445. arXiv:http://pubs.acs.org/doi/pdf/10.1021/ja805169z, doi:10.1021/ja805169z.
URL http://pubs.acs.org/doi/abs/10.1021/ja805169z

[31] R. Atkin, V. S. J. Craig, E. J. Wanless, S. Biggs, Mechanism of cationic surfactant adsorption at the solid-aqueous interface, Advances in Colloid and Interface Science 103 (2003) 219–304.

[32] R. Atkin, V. S. J. Craig, S. Biggs, Adsorption kinetics and structural arrangements of cationic surfactants on silica surfaces, Langmuir 16 (24) (2000) 9374–9380.
URL http://pubs3.acs.org/acs/journals/doilookup?in_doi=10.1021/la0001272

[33] S. C. Howard, V. S. J. Craig, Very slow surfactant adsorption at the solid-liquid interface is due to long lived surface aggregates, Soft Matter 5 (2009) 3061–3069. doi:10.1039/B903768C.
URL http://dx.doi.org/10.1039/B903768C

[34] C. C. Ruiz, J. Aguiar, Interaction, stability, and microenvironmental properties of mixed micelles of triton x100 and n-alkyltrimethylammonium bromides: Influence of alkyl chain length, Langmuir 16 (21) (2000) 7946–7953.
URL http://pubs3.acs.org/acs/journals/doilookup?in_doi=10.1021/la000154s

Supplementary Material

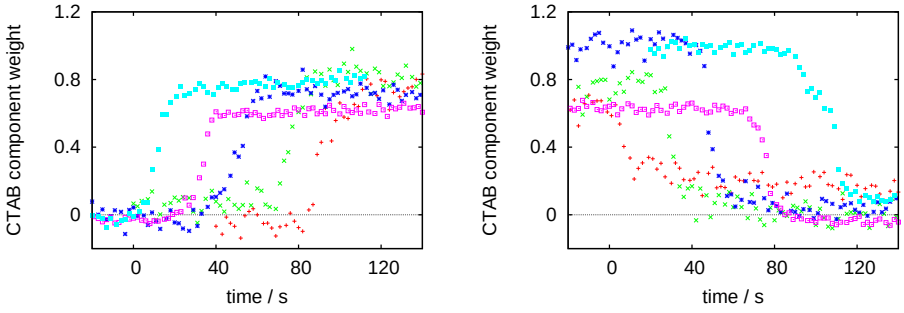

(a) (b)

Figure S.1: CTAB kinetics for 0.47 mM (red +), 0.75 mM (green ×), 1.0 mM (blue *), 4 mM (pink ⊡), 10 mM (turquoise ■). (a) Adsorption kinetics, (b) desorption kinetics. The curves have been offset on the time axis for ease of viewing. The kinetics are presented in terms of component weight (normalised to water) rather than surface excess owing to the uncertainty in the calibration factor.

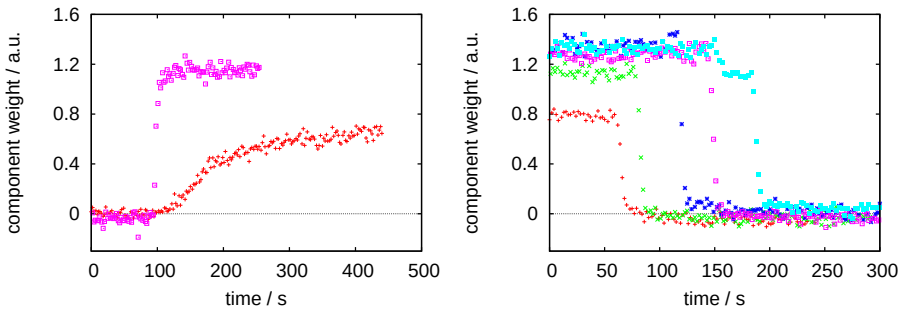

(a) (b)

Figure S.2: (a) Adsorption and (b) desorption kinetics of TX-100 onto cellulose. Concentrations are 0.2 mM (red +), 0.4 mM (green ×), 1.0 mM (blue *), 4 mM (pink ⊡) and 10 mM (turquoise ■) The different runs have been offset on the time axis for ease of viewing. The kinetics are presented in terms of component weight (normalised to water) rather than surface excess owing to the uncertainty in the calibration factor.